

Geometrical estimators as a test of Gaussianity in the CMB

R.B.Barreiro¹, E.Martínez-González² and J.L.Sanz²

¹ *Astrophysics Group, Cavendish Laboratory, Madingley Road, Cambridge CB3 0HE, UK*

² *Instituto de Física de Cantabria, Fac. Ciencias, Avda. de los Castros s/n, 39005 Santander, Spain*

Accepted ????. Received ???; in original form ???

ABSTRACT

We investigate the power of geometrical estimators on detecting non-Gaussianity in the cosmic microwave background. In particular the number, eccentricity and Gaussian curvature of excursion sets above (and below) a threshold are studied. We compare their different performance when applied to non-Gaussian simulated maps of small patches of the sky, which take into account the angular resolution and instrumental noise of the Planck satellite. These non-Gaussian simulations are obtained as perturbations of a Gaussian field in two different ways which introduce a small level of skewness or kurtosis in the distribution. A comparison with a classical estimator, the genus, is also shown. We find that the Gaussian curvature is the best of our estimators in all the considered cases. Therefore we propose the use of this quantity as a particularly useful test to look for non-Gaussianity in the CMB.

Key words: methods: statistical - cosmic microwave background

1 INTRODUCTION

Future cosmic microwave background (CMB) experiments, such as the VSA (Jones & Scott 1998), the NASA MAP satellite (Bennett et al. 1997) and the Planck mission from ESA (Tauber 2000), will provide with unique data to constraint fundamental cosmological parameters as well as to distinguish between competing theories of structure formation in the early universe. In particular, the standard inflationary model predicts Gaussian fluctuations whereas topological defects give rise to non-Gaussian signatures in the CMB. Therefore, the study of the Gaussianity of the CMB is a key issue to understand the nature of the primordial perturbations that led to the formation of large-scale structure. In addition, future high resolution maps should be searched for any traces of non-Gaussianity since both foregrounds and systematic errors can also leave non-Gaussian imprints.

A large number of methods have been proposed in the literature to test the Gaussianity of the CMB (for a review see Barreiro 2000). They include extrema correlation function (Kogut et al. 1996, Barreiro et al. 1998, Heavens & Sheth 1999), properties of hot and cold spots (Coles & Barrow 1987, Martínez-González et al. 2000), Minkowski functionals (Coles 1988, Gott et al. 1990, Kogut et al. 1996), bispectrum analysis (Ferreira et al. 1998, Heavens 1998, Magueijo 2000), wavelets (Pando et al. 1998, Hobson et al. 1999, Mukherjee et al. 2000, Barreiro et al. 2000), multifrac-

tals (Pompilio et al. 1995) and partition function (Diego et al. 1999, Martínez-González et al. 2000).

In this paper we investigate the use of geometrical estimators on detecting non-Gaussianity in the CMB using small scale simulated maps (for Gaussian and non-Gaussian fields). These simulations take into account the angular resolution and sensitivity predicted for two of the Planck frequency channels (the LFI 100 GHz and the HFI 217 GHz channels). In particular, we study the performance of the number, eccentricity and Gaussian curvature of excursion sets above (or below) a threshold. These quantities have been studied for a Gaussian field by Barreiro et al. (1997). For comparison, we also present the same analysis for the genus, a topological quantity that has been proposed as a good estimator to test the Gaussianity of the CMB.

Simulated maps for the standard inflationary model can be very accurately (at the level of $\simeq 1$ per cent in the power spectrum) obtained (e.g. Seljak & Zaldarriaga 1996, Hu et al. 1998). However this is not the case for models based on topological defects. Besides, the power spectrum predicted by pure topological defects scenarios (see e.g. Pen et al. 1997, Contaldi et al. 1999) seems not to be in agreement with the latest CMB data produced by BOOMERANG (de Bernardis et al. 2000) and MAXIMA (Hanany et al. 2000) but the possibility of an hybrid scenario that combines both inflation and topological defects remains viable (Bouchet et al. 2000, Contaldi 2000). To take into account for all of these uncertainties, we have used two *generic* non-Gaussian fields. In

particular, physically motivated non-Gaussian models, e.g. those based on topological defects or non-standard inflation, generically produce certain level of skewness or/and kurtosis. Since these are the lowest order cumulants they are also the least affected by the presence of instrumental white noise. Therefore, we have generated two different kind of non-Gaussian maps obtained as weak perturbations of a Gaussian field. The first one, that we call *P* distribution, has an asymmetric 1-point density function (1-pdf) with a positive tail, what introduces a small level of skewness. The 1-pdf of the second non-Gaussian field, the *B* distribution, is symmetric and have a higher peak and longer tails than the Gaussian one. This produces a positive value of the (excess) kurtosis. Some of these characteristics have been shown to be produced by topological defect models by different authors. Turok (1996) performed sub-degree scale simulations of the CMB from cosmic defects, finding a clear excess of hot spots for monopoles and textures, a signature also present on our *P* distribution. Perivolaropoulos (1993) used an analytical model to investigate the statistics of the CMB temperature maps induced by topological defects. He obtained a 1-pdf for cosmic strings that presents a central peak and long tails, resembling our *B* distribution.

The outline of this paper is as follows. In §2 we discuss the geometrical quantities that we test as non-Gaussian estimators. §3 describes our Gaussian and non-Gaussian CMB simulations. The results, including the effect of instrumental noise, are presented in §4. Finally, the main conclusions of our work are summarised in §5.

2 GEOMETRICAL ESTIMATORS

We have already pointed out the importance of testing the Gaussianity of the CMB. An interesting possibility is the use of geometrical estimators related to excursion sets above or below a given threshold. In particular, we have considered the mean number, eccentricity and Gaussian curvature of regions above or below a threshold ν (in units of the signal dispersion). All these quantities can be easily estimated from a map. The procedure is as follows. First the excursion sets, i.e. connected pixels, above ν (and below $-\nu$) are identified. Each of them is fitted to a paraboloid with parameters a , b and c (see Fig. 1). The eccentricity ε and Gaussian curvature κ of each of the spots are then estimated as

$$\begin{aligned} \varepsilon &= \sqrt{1 - \left(\frac{b}{a}\right)^2} \\ \kappa &= \frac{c}{ba} \end{aligned} \quad (1)$$

where a, b are in arcminutes and c in units of the map dispersion. Only those excursion sets with a single maximum (or minimum when below the threshold) and formed by at least eight pixels are considered to obtain the mean Gaussian curvature and eccentricity of the map.

In addition, these quantities can be obtained (semi)analytically for a homogeneous and isotropic Gaussian field, at least locally around the maximum. On the one hand, the probability density functions of the number, eccentricity and Gaussian curvature of maxima (which coincide asymptotically with the excursion sets) for a homogeneous and isotropic Gaussian field have been studied

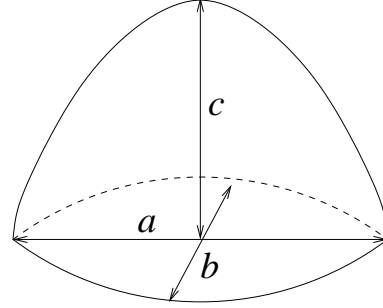


Figure 1. To obtain the mean eccentricity and Gaussian curvature of the excursion sets of the CMB, these are fitted to a paraboloid as the one shown in the figure. a and b are the major and minor axes of the ellipse that forms the basis. c is the distance between the geometrical centre of the ellipse and the maximum of the paraboloid

by Barreiro et al. (1997). On the other hand, the expected number of excursion sets $\langle N \rangle$ over the whole sphere can be estimated as (Vanmarcke 1983):

$$\langle N \rangle = \frac{2}{\pi\theta_c^2} \frac{e^{-\nu^2}}{\operatorname{erfc}(\nu/\sqrt{2})} \quad (2)$$

where θ_c is the coherence angle of the field that depends only on the 2-point correlation function.

For comparison, we have also extended our analysis to the genus, a topological quantity that has been commonly used to test the Gaussianity of the CMB. The genus at a given threshold can be approximately estimated as the number of isolated high-temperature regions minus the number of isolated low-temperature regions. The mean genus $\langle g \rangle$ per unit area for a homogeneous and isotropic Gaussian field is given by

$$\langle g \rangle = \frac{1}{(2\pi)^{3/2}\theta_c^2} \nu e^{-\nu^2/2} \quad (3)$$

To estimate this quantity from a map we have used a method based on adding up the contribution to the genus from each vertex of the pixelised map. This method is described in detail in Jones (1999) (see also Hamilton et al., 1986).

In order to study the validity of our algorithms on estimating the above quantities, we have compared the values computed from simulations with the theoretical expectations for the Gaussian case. Fig. 2 shows the mean number of regions, eccentricity, the inverse of the Gaussian curvature and genus obtained from 500 Gaussian realisations for a Λ -CDM model. The size of the maps is 512×512 pixels, with a pixel size of $1'.5$ and they have been smoothed with a Gaussian beam of $\text{FWHM} = 5.5$. The solid lines correspond to an approximation of the theoretical expectations for each of these quantities. For the number of regions and genus, the curves have been obtained from equations 2 and 3 respectively, whereas the inverse of the Gaussian curvature and the eccentricity were calculated using the probability density functions given by Barreiro et al. (1997). We can see that there is a certain difference between the computed and predicted values for the number of regions, especially at low thresholds. This is due to the fact that the Vanmarcke conjecture is an approximation that overestimates the number

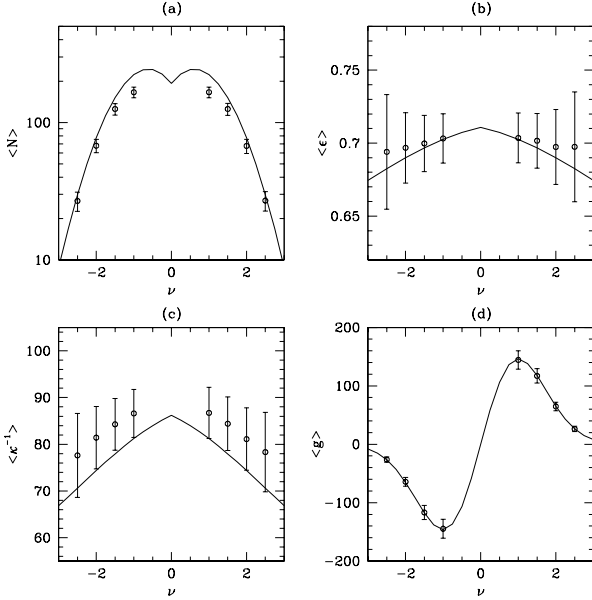


Figure 2. Comparison of the average values of our estimators as computed from 500 simulated maps (open circles) with an approximation of the theoretical expectations for a Gaussian field (solid lines). The error bars show the dispersion obtained from the simulations. The panels correspond to (a) number of regions, (b) eccentricity and (c) inverse of the Gaussian curvature for excursion sets above (or below for negative ν) a threshold ν , and (d) genus.

of excursion sets at low thresholds. Regarding the inverse of the Gaussian curvature as well as the eccentricity, we have to point out that the theoretical values have been obtained locally around the maxima, whereas on the simulations we consider the whole of the excursion set and discard those with more than a single maximum and less than eight pixels. This procedure biases the expected values and can explain the discrepancies between the theoretical and computed values, that are however reasonably close. Finally, as expected, the values computed from the simulations for the genus are in good agreement with the theoretical curve.

3 SIMULATIONS

In order to test the performance of our estimators, we have simulated small patches of the sky of size 12.8 square degrees with Gaussian and non-Gaussian statistical properties. We have considered two different angular resolutions that correspond approximately to two of the Planck frequency channels. On the one hand, we have produced maps with pixel size of 3 arcminutes, smoothed with a Gaussian beam of $\text{FWHM}=10'$, which corresponds to the resolution of the LFI 100 GHz channel. On the other hand, we have simulated maps with the characteristics of the HFI 217 GHz channel, i.e., pixel size of 1.5 arcminutes and Gaussian beam of $\text{FWHM}=5'.5$. We have also taken into account the instrumental noise of these channels.

The Gaussian simulated maps have been generated from

a CDM model normalised to COBE/DMR and parameters $\Omega_m = 0.3$, $\Omega_\Lambda = 0.7$, $h = 0.5$, $\Omega_b = 0.05$ and $n = 1$. The power spectrum of such a model has been obtained with CMBfast (Seljak & Zaldarriaga 1996). The non-Gaussian simulations have been produced as follows. First, an uncorrelated 2D Gaussian map with zero mean and unit variance is obtained. This map is then transformed in two different ways according to the following expressions (Weinberg & Cole 1992):

$$F_1 = \frac{e^{aG} - e^{a^2/2}}{\sqrt{e^{2a^2} - e^{a^2}}} \quad P \text{ transformation} \quad (4)$$

$$F_2 = \frac{G(e^{aG} + e^{-aG})}{\sqrt{2[1 + (1 + 4a^2)e^{2a^2}]}} \quad B \text{ transformation} \quad (5)$$

where G corresponds to the initial Gaussian field and F_1, F_2 to the transformed fields. The level of non-Gaussianity introduced can be controlled with the parameter a . In particular when $a \rightarrow 0$ we recover the Gaussian case. In this way, we obtain two kind of uncorrelated non-Gaussian fields with zero mean and unit variance. Next, we rescale the amplitude of each Fourier mode to obtain the same power spectrum as for the Gaussian CDM model. By rescaling the power spectrum the 1-pdf is modified with respect to the uncorrelated one, but it is still non-Gaussian (hereinafter, when we refer to P and B transformations, it should be understood the transformations given by (4) and (5) plus a subsequent rescaling of the power spectrum as explained before). In particular, for the P transformation we are constructing a non-Gaussian field whose distribution is skewed with a positive tail, whereas for the B transformation, the distribution is broadened with both positive and negative tails. Finally, the new maps are smoothed with the required Gaussian beam. For both kind of non-Gaussian fields, we have considered small enough values of a such that their 1-point distributions are indistinguishable from the Gaussian one. In addition, the Gaussian and non-Gaussian simulations share the same power spectrum by construction. Fig. 3 (top panels) shows the 1-pdf for the Gaussian and non-Gaussian fields for $a = 0.8$ that have been obtained averaging over 500 simulations with angular resolution corresponding to the 217 GHz channel. Noise has not been included in this case. For the sake of clarity, we have not plotted the value of the dispersion at each bin of the histogram as error bars but they completely overlap for the Gaussian and non-Gaussian 1-pdf's. We can see that the P distribution has a positive skewness, whereas the B one presents a small level of kurtosis. This can also be seen in the middle and bottom panels, where the histogram of the values of the skewness and kurtosis have been plotted for the 500 Gaussian and non-Gaussian simulations (these quantities have been obtained using unbiased estimators as explained in Hobson et al. 1999). Table 1 gives the average values as well as the dispersions of the skewness and kurtosis distributions obtained from the previous simulations. From these values, we can see that the Gaussian and non-Gaussian distributions can be differentiated only at the $\sim 1\sigma$ level using the skewness and kurtosis.

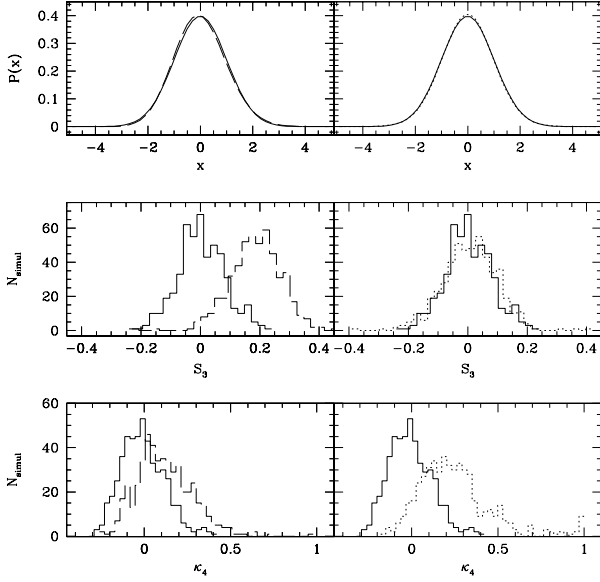


Figure 3. Top: 1-pdf function for the Gaussian (solid line), P (dashed line) and B (dotted line) distributions (with unit dispersion) obtained averaging over 500 simulations. The parameter $a = 0.8$ has been used for the transformed fields. The size of the simulated maps was 12.8 square degrees with a pixel of 1.5 arcminutes and they were smoothed with a Gaussian beam with FWHM=5.5 arcminutes, which corresponds to the angular resolution of the Planck 217 GHz channel. The corresponding histograms for the skewness (middle) and kurtosis (bottom) for the same simulations are also plotted.

Table 1. Values of the mean and dispersion of the skewness and kurtosis distributions obtained from 500 simulations.

Distribution	$\langle S_3 \rangle$	$\sigma(S_3)$	$\langle K_4 \rangle$	$\sigma(K_4)$
G	3.72×10^{-3}	7.80×10^{-2}	-6.55×10^{-3}	0.125
P ($a=0.8$)	0.188	8.60×10^{-2}	0.117	0.161
B ($a=0.8$)	7.35×10^{-3}	9.30×10^{-2}	0.270	0.358

4 RESULTS

In order to compare the power of our estimators, we have obtained the mean number, eccentricity, Gaussian curvature and genus for a large number of Gaussian and non-Gaussian simulations with two different angular resolutions which correspond to the LFI 100 GHz and the HFI 217 GHz channels of the Planck satellite. We have chosen a value of $a = 0.8$ for the non-Gaussian maps, that introduces small but interesting differences. We have also investigated the effect of instrumental noise. In order to have a reasonable number of spots at any given threshold in all of our realisations we have considered thresholds in the range $-2.5 \leq \nu \leq 2.5$ ($-2 \leq \nu \leq 2.5$ for the P distribution in some cases). In most of our cases thresholds close to $\nu = 0$ do not contain very relevant information and have not been included to speed up the numerical calculations.

4.1 Noiseless case

First we will consider simulated maps where no noise has been included. The top panels of Fig. 4a show the mean value and dispersion of the number of spots above (for positive ν) or below (for negative ν) a threshold obtained over 500 Gaussian and non-Gaussian realisations of size 256×256 (pixel $3'$) and smoothed with a Gaussian beam of FWHM= $10'$ (LFI 100 GHz channel). Open circles, solid triangles and solid squares correspond to the Gaussian, P and B fields respectively. In order to establish a better comparison we have constructed the likelihood function for the Gaussian and non-Gaussian maps (compared to the Gaussian model) given by

$$L = \frac{1}{\sqrt{2\pi}|M|^{1/2}} e^{-\frac{1}{2}(x^s - \langle x^G \rangle)^T M^{-1} (x^s - \langle x^G \rangle)}, \quad (6)$$

$$M_{ij} = \langle (x_i^G - \langle x_i^G \rangle)(x_j^G - \langle x_j^G \rangle) \rangle$$

where s refers to the Gaussian and non-Gaussian simulated data and G to the Gaussian ones. M is computed from the Gaussian realisations. The histogram of the likelihood values for our Gaussian and non-Gaussian fields when using the number of spots are plotted in the bottom panels of Fig. 4a. The mean values, dispersions and likelihood curves for the eccentricity, Gaussian curvature and genus (in absolute value) are given in Figs. 4b, 4c and 4d respectively. For negative thresholds the Gaussian curvature and eccentricity correspond to the excursion sets below that threshold. We can see in these figures that the P distribution can be clearly distinguished from the Gaussian model using the number, Gaussian curvature or the genus since the likelihood curves do not overlap, whereas the eccentricity does not discriminate between both distributions. In the three first cases, the 100% of the non-Gaussian simulations lie outside the Gaussian 99% confidence limit of the Gaussian case, whereas only 23.8% of the P simulations could be distinguished from the Gaussian model at the 99% c.l. using the eccentricity. To establish a better comparison in the performance of our estimators, we have calculated a factor d defined as

$$d = \frac{m_G - m_{NG}}{\sigma_G} \quad (7)$$

where m_G and m_{NG} correspond to the median of the likelihood curve of the Gaussian and non-Gaussian cases respectively and σ_G is the dispersion of the likelihood curve for the Gaussian simulations. Therefore this quantity is an indication of how well we can separate between the Gaussian and non-Gaussian distribution with a given estimator. Table 2 gives the values of this quantity for the different cases considered in this paper without including instrumental noise. In the same table, the quantity f indicates the percentage of non-Gaussian simulations that lies outside the Gaussian 99% c.l. for a given estimator. We can see that for the P distribution in the case of the LFI 100 GHz channel, the highest value of d (and therefore the best estimator) corresponds to the Gaussian curvature ($d=44.8$ versus $d=24.7$ for the genus, the next best quantity). Regarding the B model, the likelihood curves overlap for all the estimators, except for the Gaussian curvature, that gives again the best results ($d=26.1$, $f=100\%$). The other three estimators can not discriminate between both distributions, being the eccentricity ($d=3.9$, $f=60.6\%$) slightly better than the genus ($d=3.4$, $f=56.2\%$) and the number ($d=2.6$, $f=45.8\%$).

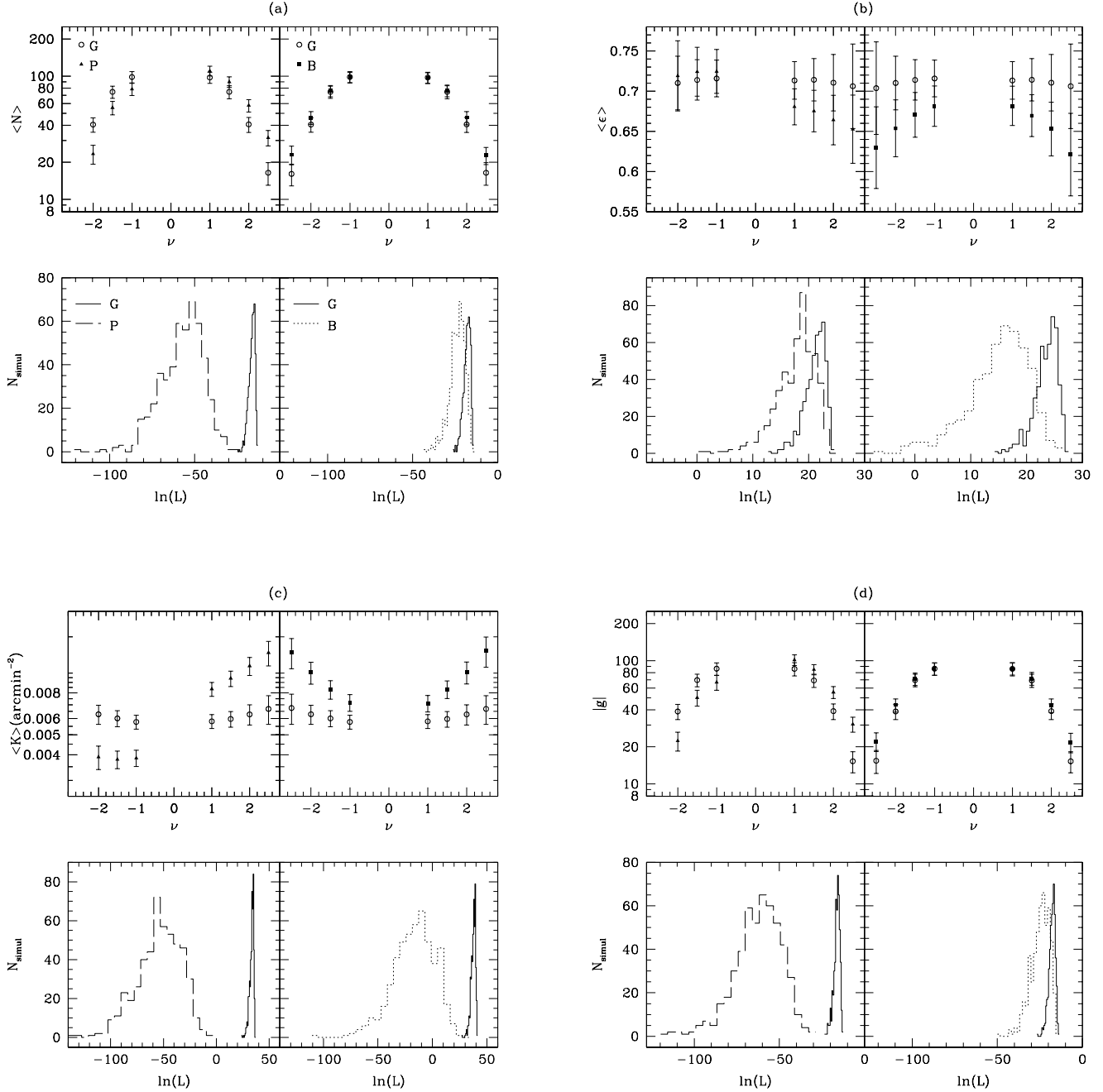


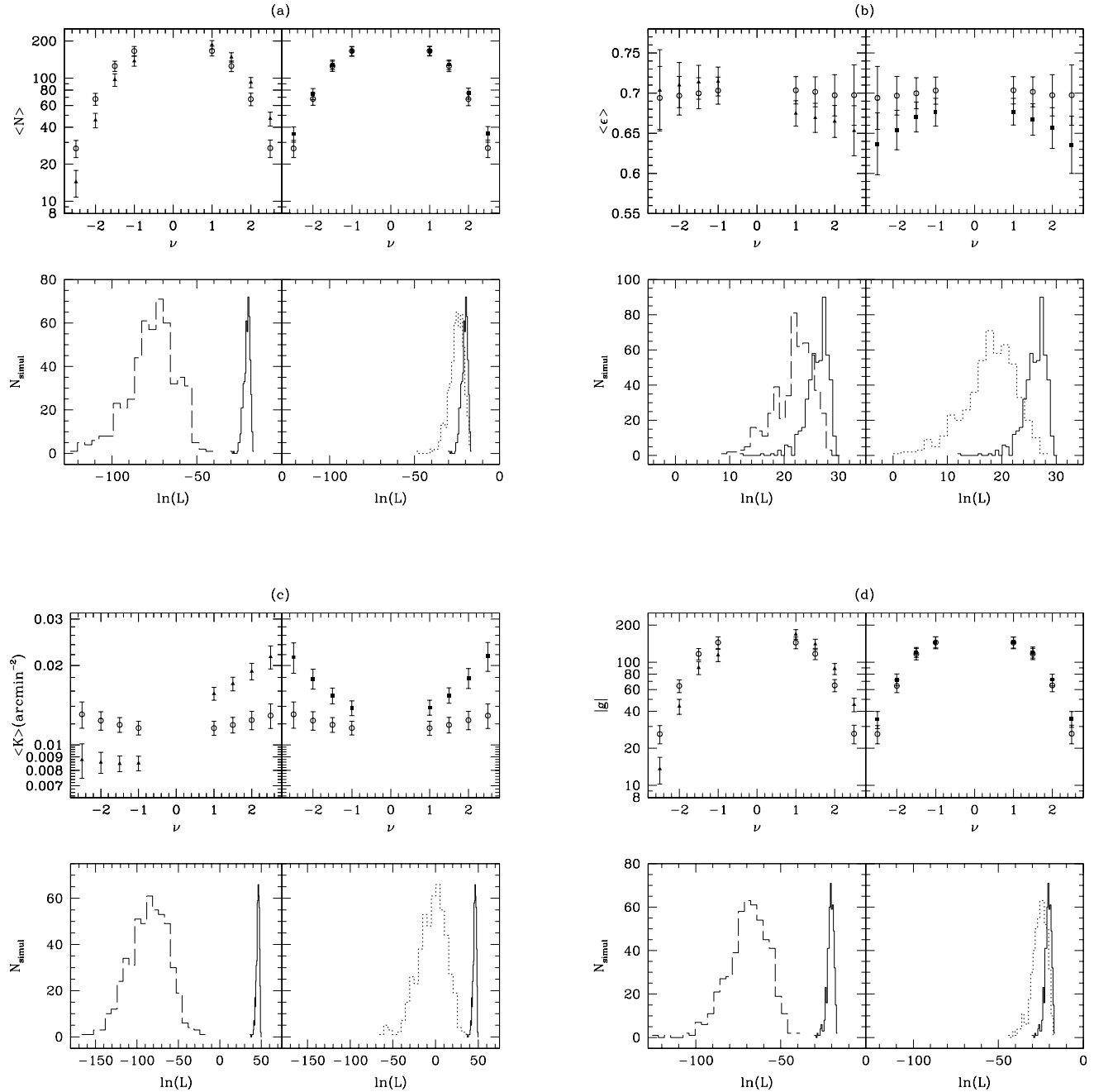
Figure 4. A comparison of the power of our estimators on detecting small scale non-Gaussianity using simulated maps with the specifications of the Planck 100 GHz channel (no noise) is shown. The four figures in the top-left corner (labelled (a)) correspond to the results for the number of spots above (for positive thresholds) or below (for negative thresholds) ν . The two top figures of this set show the mean values and dispersions obtained from the distribution of the number of excursion sets over 500 simulations for the Gaussian (open circles), P (solid triangles) and B (solid squares) fields. The histogram of likelihood values computed from the same simulations are plotted in the two corresponding bottom figures for the Gaussian (solid line), P (long-dashed line) and B (short-dashed line) distributions. The same results are given for the eccentricity (top-right figures, labelled (b)), Gaussian curvature (lower-left figures, (c)) and genus (lower-right figures, (d)).

The results for the small simulated maps of the 217 GHz channel (512×512 maps, pixel= $1'.5$, FWHM= $5'.5$) are shown in Figs. 5a (number), 5b (eccentricity), 5c (curvature) and 5d (genus). As before, the P distribution can

be clearly distinguished from the Gaussian one using the Gaussian curvature, genus or number of excursion sets but not with the eccentricity. In particular the Gaussian curvature is again the best of our statistics with $d=67.1$ and $f=100\%$ whereas the mean number ($d=28.5$, $f=100\%$) and genus ($d=24.1$, $f=100\%$) produce very similar results. The

Table 2. Values of d and f (no noise)

Channel	Factor	P distribution				B distribution			
		N	ε	κ	g	N	ε	κ	g
100 GHz	d	21.6	1.6	44.8	24.7	2.6	3.9	26.1	3.4
	$f(\%)$	100	23.8	100	100	45.8	60.6	100	56.2
217 GHz	d	28.5	2.0	67.1	24.1	2.5	3.9	24.9	2.4
	$f(\%)$	100	23.4	100	100	41.6	58.4	100	36.0

**Figure 5.** As in Fig.4, but with the results corresponding to the 217 GHz channel.

$\langle \kappa \rangle$ also succeeds in distinguishing between the B and Gaussian distributions ($d=24.9, f=100\%$), failing the rest of estimators to discriminate between them.

It is interesting to point out that, in spite of the better resolution of the 217 GHz channel, the level of success of our estimators is very similar for both the 100 and 217 GHz channels. This can be understood taking into account that the coherence angle for the considered Λ -model is $\simeq 10'$. Therefore the information about the intrinsic structure of the CMB contained in both channels is very similar.

4.2 The effect of instrumental noise

We have also investigated the effect of instrumental noise in the performance of our estimators. In particular, we have included white Gaussian noise at the level predicted for the Planck satellite after 12 months of observation for the two channels that we are considering ($\Delta T/T$ per resolution element = 4.3×10^{-6} in both cases). For our model this corresponds to a signal to noise ratio (S/N) per pixel of $S/N \simeq 2.8$ and $S/N \simeq 2.7$ for the 100 and 217 GHz channels respectively. In order to increase the S/N , the simulated signal plus noise maps have been smoothed with a Gaussian beam with FWHM equal to the antenna of the corresponding channel.

The results are summarised in Table 3 and Figs. 6a (Gaussian curvature, 100 GHz), 6b (genus, 100 GHz), 6c (Gaussian curvature, 217 GHz) and 6d (genus, 217 GHz). Only the two best estimators are shown. The most interesting point is that again the Gaussian curvature is the best estimator in all the considered cases. In particular for the P distribution the 100% of the realisations have lied outside the 99% confidence level of the Gaussian model for both frequency channels. The genus and the number of excursion sets give again very similar results. They are able to discriminate between most of the P and Gaussian realisations, although the confusion level is larger than for the Gaussian curvature. The eccentricity completely fails to distinguish between them.

For the B distribution, there is a small overlap between both likelihood curves when using the Gaussian curvature but still most of the realisations fall outside the Gaussian 99% c.l. ($d=6.8, f=93\%$ for the 100 GHz channel, $d=8.2, f=89\%$ for the 217 GHz channel). The number, genus and eccentricity can not discriminate between the B and Gaussian distributions having values of $d \sim 1$.

5 CONCLUSIONS

We have performed a comparative study of the ability of three geometrical estimators (mean number, eccentricity and Gaussian curvature of excursion sets above or below a threshold) as well as the genus on detecting small scale non-Gaussianity in the CMB. To test such estimators, we have generated two kind of non-Gaussian realisations that are perturbations of a Gaussian field. The first one (P distribution) introduces a certain level of skewness in the 1-pdf whereas the second one (B distribution) has a non-negligible kurtosis. This could resemble the characteristics of some topological defect models. The simulated maps are small

patches of the sky (12.8 square degrees) with angular resolutions which correspond approximately to two of the Planck satellite frequency channels, the LFI 100 GHz channel (pixel size of $3'$, FWHM= $10'$) and the HFI 217 GHz (pixel size of $1'.5$, FWHM= $5'.5$). We have also taken into account the expected level of instrumental noise in these channels.

We find that the Gaussian curvature is the best of our estimators. This is a robust conclusion, since this quantity performs considerably better than the genus, number and eccentricity of excursion sets for both types of non-Gaussian fields, in presence or absence of noise and for the two considered angular resolutions. Regarding the number of excursion sets and the genus, these two quantities carry very similar information, as one would expect. They can discriminate between the P and Gaussian models at a fairly high level (although always worse than the Gaussian curvature) in all the considered cases. However, these quantities fail to discriminate between the B and Gaussian distributions, being the level of confusion especially high when instrumental noise is introduced. The performance of the eccentricity is very poor. In none of the considered cases can clearly discriminate between the non-Gaussian and Gaussian fields, although it is interesting to point out that it does perform at similar or better levels than the genus and the number of excursion sets when testing the B distribution. Therefore, the main conclusion of our work is that the mean Gaussian curvature of excursion sets could be a very useful estimator to look for small scale non-Gaussianity in the CMB.

ACKNOWLEDGEMENTS

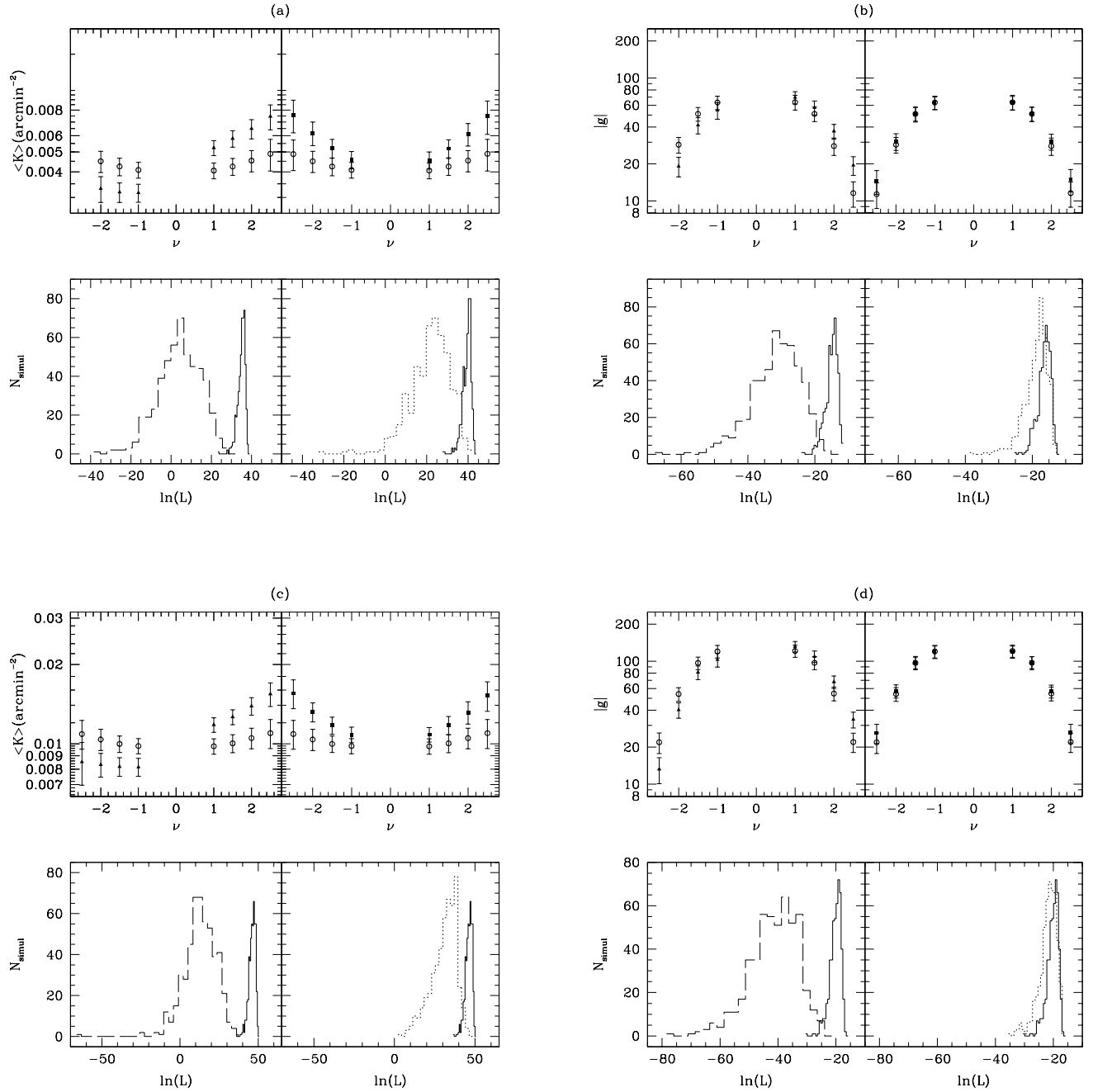
The authors warmly thank Laura Cayón, Jose M. Diego, Pedro Ferreira, Aled Jones and Mike Hobson for useful discussions related to this work. RBB acknowledges financial support from the PPARC in the form of a research grant. EMG and JLS thank the Comisión Conjunta Hispano-Norteamericana de Cooperación Científica y Tecnológica ref. 98138, Spanish DGEIC Project no. PB98-0531-c02-01, FEDER project no. 1FD97-1769-c04-01 and the EEC project INTAS-OPEN-97-1992 for partial financial support. RBB thanks the Instituto de Física de Cantabria for its hospitality during a stay in 2000.

REFERENCES

- Barreiro R.B., 2000, *New Astron. Rev.*, 44, 179
- Barreiro R.B., Hobson M.P., Lasenby A.N., Banday A.J., Górski K.M. & Hinshaw G., 2000, *MNRAS*, in press
- Barreiro R.B., Sanz J.L., Martínez-González E., Cayón L. & Silk J., 1997, *ApJ*, 478, 1
- Barreiro R.B., Sanz J.L., Martínez-González E., & Silk J., 1998, *MNRAS*, 296, 693
- Bennett C.L. et al., 1997, *AAS*, 191, 8701; MAP homepage <http://map.gsfc.nasa.gov>
- Bouchet F.R., Peter P., Riazuelo A. & Sakellariadou, 2000, *Phys.Rev.Lett.*, submitted (astro-ph/0005022)
- Coles P. & Barrow J.D., 1987, *MNRAS*, 228, 407
- Coles P., 1988, *MNRAS*, 234, 509
- Contaldi C.R., 2000, *Phys.Rev.Let.*, submitted (astro-ph/0005115)
- de Bernardis, P. et al., 2000, *Nature*, 404, 955

Table 3. Values of d and f (noise included)

Channel	Factor	P distribution				B distribution			
		N	ε	κ	g	N	ε	κ	g
100 GHz	d	7.5	0.4	16.2	8.9	0.9	0.8	8.2	1.0
	$f(\%)$	93.6	5.0	100	97.6	12.4	10.0	89.0	19.8
217 GHz	d	11.4	1.1	16.4	10.5	0.9	1.5	6.8	0.7
	$f(\%)$	99.6	7.0	100	99.2	10.0	12.0	93.0	11.4

**Figure 6.** The results for the Gaussian curvature-100 GHz (four top-left figures, (a)), genus-100 GHz (top-right figures, (b)), Gaussian curvature-217 GHz (bottom-left figures, (c)) and genus-217 GHz (bottom-right, (d)) are shown. Noise has been included in the simulations.

- Diego J.M., Martínez-González E., Sanz J.L., Mollerach S. & Martínez V.J., 1999, 306, 427
- Ferreira P.G., Magueijo J. & Górski K.M., 1998, ApJ, 503, L1
- Gott III J.R., Park C., Juszkiewicz R., Bies W.E., Bennett D.P., Bouchet F.R. & Stebbins A., 1990, ApJ, 352, 1
- Hamilton A.J.S., Gott III J.R. & Weinberg D., 1986, ApJ, 309, 1
- Hanany S. et al., 2000, ApJL, submitted (astro-ph/0005123)
- Heavens A.F., 1998, MNRAS, 299, 805
- Heavens A.F. & Sheth R.K., 1999, MNRAS, 310, 1062
- Hobson M.P., Jones A.W. & Lasenby A.N., 1999, MNRAS, 309, 125
- Hu W., Seljak U., White M. & Zaldarriaga M. 1998, Phys.Rev., D57, 3290
- Kogut A., Banday A.J., Bennett C.L., Górski K., Hinshaw G., Smoot G.F. & Wright E.L., 1996, ApJ, 464, L29
- Jones A.W., 1998, 'Application of novel analysis techniques to Cosmic Microwave Background Astronomy', PhD thesis, U.Cambridge
- Jones M.E. & Scott P.F. 1998, in J.Trân Thanh Vân, et al. (Eds.), Fundamental Parameters in Cosmology, Proc. of the XXXII-Ird Recontres de Moriond (France), Editions Frontières, p.233
- Magueijo J., 2000, ApJ, 528, L57 (see also Magueijo J., 2000, ApJ, 532, L157)
- Martínez-González E., Barreiro R.B., Diego J.M., Sanz J.L., Cayón L., Silk J., Mollerach S. & Martínez V.J., 2000, ApL&C, in press
- Mukherjee P., Hobson M.P. & Lasenby A.N., 2000, MNRAS, in press (astro-ph/0001385)
- Pando J., Valls-Gabaud D. & Fang L., 1998, Phys.Rev.Lett., 81, 4568
- Perivolaropoulos L., 1993, Phys.Rev., D48, 1530
- Pompilio M.P., Bouchet F.R., Murante G. & Provenzale A., 1995, ApJ, 449, 1
- Seljak U. & Zaldarriaga M., 1996, ApJ, 469, 437
- Tauber J.A., 2000, ApL&C, in press; Planck homepage <http://astro.estec.esa.nl/Planck/>
- Turok N., 1996, ApJ, 473, L5
- Vanmarcke E.H., 1983, 'Random fields: Analysis and Synthesis', MIT Press, Cambridge, MA